Full Paper

Propellants, Explosives, Pyrotechnics

DOI: 10.1002/prep.201300026

Effect of Al/O Ratio on the Detonation Performance and Underwater Explosion of HMX-based Aluminized Explosives

Da-Lin Xiang,[a] Ji-Li Rong,*[a] and Jian Li[b]

Abstract: The performance of detonation and underwater explosion (UNDEX) of a six-formula HMX-based aluminized explosive was examined by detonation and UNDEX experiments. The detonation pressures, detonation velocities, and detonation heat of HMX-based aluminized explosive were measured. The reliability between the experimental results and those calculated by an empirical formula and the KHT code was verfied. UNDEX experiments were carried out on the propagation of a shock wave and a bubble pulse of a 1 kg cylindrical HMX-based aluminized explosive underwater at a depth of 4.7 m. Based on the experimental results of the shock wave, the coefficients of similarity law equation for the peak pressure and attenuation time constant of shock wave were in acceptable agreement. The bubble motion during UNDEX was simulated using MSC.DYTRAN software, and the radius–time curves of bubbles were determined. The effect of the aluminum/oxygen ratio on the performance of the detonation and UNDEX for an HMX-based aluminized explosive was discussed.

Keywords: HMX-based aluminized explosive · Aluminum-oxygen ratio(Al/O ratio) · Detonation parameters · Underwater explosion · Aluminum particle

1 Introduction

The chemical energy of an explosive detonated underwater can be converted into three parts, namely, shock wave energy, bubble energy, and heat energy loss due to the compression of the aqueous medium [1]. The proportion of the three parts of energy distribution and attenuation variation when propagating in water has to be taken into account for the design of explosives with different underwater energy output structures. Generally, scientists are concerned about the explosives' thermochemical properties and the relationship between the formula and detonation performance, such as empirical formulas of detonation [2–5] and well-known equations of state (EOS) of detonation products: BKW-EOS [6], JCZ-EOS [7], KHT-EOS [8], and JWL-EOS [9]. On the other hand, they are usually more focused on the underwater damage effects of explosives [10–20] and there is a connection between formula, detonation performance and underwater damage effect. Therefore, research on the exact relationship between the damage effect of aluminized explosive and underwater energy output structure is necessary to optimize the design of charge for underwater weapons.

According to the US Office of the Naval Research, analysis of the effect of formula on the energy output structure, and the set-up of a set of formula to calculate the shock wave and bubble energy are necessary to explore the characteristics of the transition from chemical energy to shock wave energy, especially when an explosive is detonated in water [5]. Therefore, a study on the energy output structure of aluminized explosives was conducted. Swisdak [21] examined the variation of shock wave energy and bubble energy with changing aluminum/oxygen (Al/O) ratio in TNT/RDX/AL and found that with an increase in the Al/O ratio, the shock wave energy initially increases, reaches a maximum when the Al/O ratio equals to 0.4, and then gradually decreases, whereas the bubble energy continuously increases. Stromsoe and Eriksen [22] performed a set of UNDEX experiments using RDX/AL. Their experimental results suggest that when the Al/O ratio fluctuates between 0.3 and 0.4, the shock wave energy reaches a maximum value, and when the aluminum powder further increases, the shock wave energy decreases but the bubble energy continuously increases. Masahiko [23] conducted an experimental study on the underwater energy distribution of HMX/AL/PU using a small amount of charge and calculated the detonation parameters using the KHT code. The experi-

[a] *D.-L. Xiang, J.-L. Rong*
School of Aerospace Engineering
Beijing Institute of Technology
Beijing100081, P. R. China
**e-mail: rongjili@bit.edu.cn*

[b] *J. Li*
Department of Automobile Engineering
GuangxiUniversity of Technology
Liuzhou Guangxi 545006, P. R. China

mental results are in agreement with those of Keicher [24] and point out that the energy output structure is not only related to the Al/O ratio but also to the size of the aluminum particles, the oxidation capacity of the explosive and chemical thermodynamics. The role of other oxidants in explosives, such as NH_4ClO_4, should also be considered.

Although experiments have provided evidence for an effect of aluminum particles on the detonation properties of some aluminized explosives, a quantitative assessment of UNDEX performance cannot be made in absence of an appropriate experimental strategy for HMX-based aluminized explosives. This study aims to investigate the effect of the Al/O ratio on the detonation performance and UNDEX of an HMX-based aluminized explosive. To obtain the detonation parameters, detonation experiments were set-up and detonation parameters were determined using the KHT code [8]. The shock wave pressures were measured by sensors in the UNDEX experiments, and the bubble pulsation was simulated using the MSC.DYTRAN software. The results generated were considered significant for further studies in related fields.

2 Detonation Experiment

2.1 Explosive Specimen

Cylindrical pressed explosives were used in the detonation tests. The aluminum particles in the charges were grainy and evenly distributed, had no pre-oxidation treatment, and had a diameter of about 13 μm. With constant diameter and height of the charge, different sizes of HMX-based aluminized explosives were pressed fitted with 250 MPa pressure according to the detonation test requirements for pressure, velocity, and heat. The detailed formulas of HMX-based aluminized explosives are shown in Table 1.

2.2 Experimental Method

A manganin high-pressure sensor was used to measure the detonation pressure of HMX-based aluminized explosives according to the military standard in China (GJB772A-97 704.2). The schematic experimental setup is presented in Figure 1. After detonating the explosives, a shock wave, which moved at high-speed and generated high-pressure, formed. Once it hits the probe, the sensor was triggered and began to collect the voltage signal. It produced a voltage change because of the resistance change. The detonation pressure of the explosives was obtained according to the calibration relationship between voltage and pressure.

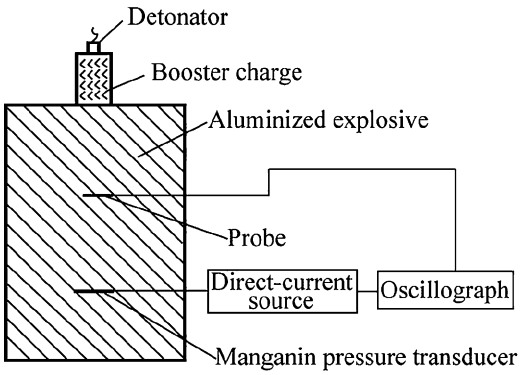

Figure 1. Experimental setup for detonation pressure measurements.

The detonation velocity of HMX-based aluminized explosives was measured by ionization probes method based on the military standard in China (GJB772A-97 702.1), a schematic of the experimental setup is shown in Figure 2. The unconfined charges were initiated by a flame detonator, and the time across the distance between each two probes was recorded by a chronoscope. The detonation velocity was calculated from the measured time interval and corresponding distance traveled by the detonation wave.

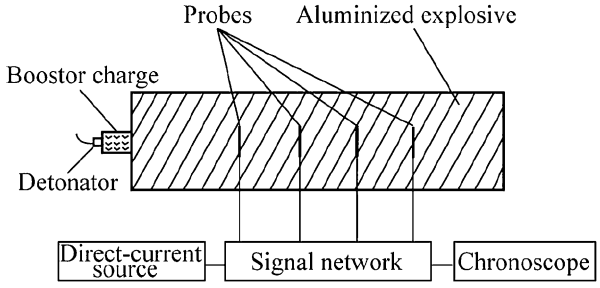

Figure 2. Experimental setup for detonation velocity measurements.

Table 1. Formulas of HMX-based aluminized explosives.

Formula No.	Al/O	Proportion [wt-%]				Density ρ [g cm^{-3}]	Average molecular formula
		HMX	Al	Wax	Graphite		
0	0	100	0	0	0	1.905	$C_4H_8N_8O_8$
1	0	95	0	3	2	1.721	$C_{1.662}H_{3.014}N_{2.566}O_{2.566}$
2	0.161	85	10	3	2	1.781	$C_{1.527}H_{2.744}N_{2.296}O_{2.296}Al_{0.371}$
3	0.366	75	20	3	2	1.844	$C_{1.392}H_{2.474}N_{2.026}O_{2.026}Al_{0.7416}$
4	0.633	65	30	3	2	1.905	$C_{1.257}H_{2.204}N_{1.756}O_{1.756}Al_{1.112}$
5	0.997	55	40	3	2	1.971	$C_{1.122}H_{1.933}N_{1.486}O_{1.486}Al_{1.483}$
6	1.523	45	50	3	2	2.029	$C_{0.987}H_{1.663}N_{1.215}O_{1.215}Al_{1.854}$

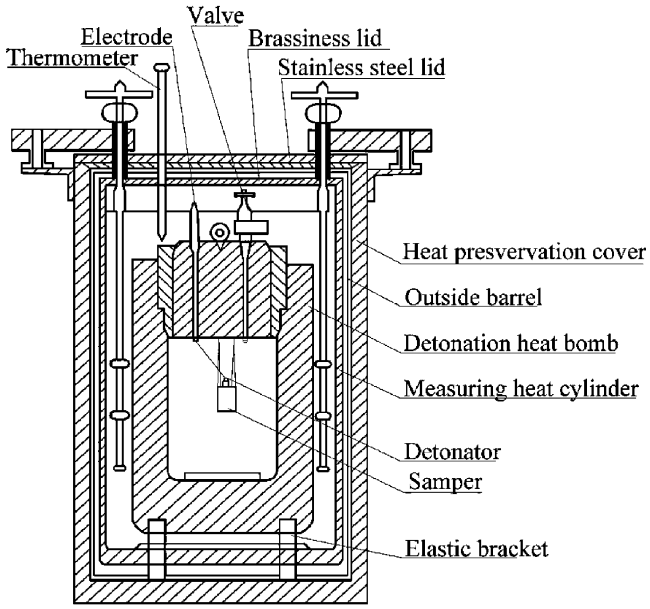

Figure 3. Sketch of the constant temperature calorimeter.

The explosion heat was measured in a detonation heat bomb according to the military standard in China (GJB772A-97 704.2), the experimental setup is presented in Figure 3. The sample was loaded into the vacuumed detonation heat bomb, which was placed in a measuring heat cylinder, and distilled water was added (1 kg). The temperatures of the measuring heat cylinder and the outer barrel were adjusted. When the temperature of the water inside and outside the barrel stabilized, a temperature t_1 was recorded. The sample was detonated, resulting in a temperature increase. The heat generated from the explosion was released to the bomb wall and transferred to the water. After obtaining a stable temperature, a temperature t_2 was recorded. The explosion heat was calculated according to Equation (1):

$$Q_v = \frac{Q_{vw} m_w (t_2 - t_1) - Q_{vd} m_d}{m_e} \quad (1)$$

where Q_v and Q_{vd} are the explosion heat of the sample and detonator, respectively [J g^{-1}]; C_v is the specific heat of the measurement systems [J g^{-1} K^{-1}]; m_w, m_d, and m_e are the mass of water, detonator, and explosive sample, respectively [g].

2.3 Detonation Parameters

The detonation pressure and velocity of aluminized explosives with general formula $C_aH_bN_cO_dAl_e$ can be determined with the empirical Equations below [3]:

$$P_{CJ} = -3.5531a + 4.1422b - 1.4770c + 4.4004d - 2.1320e + 4.3950\rho \quad (2)$$

$$D = -582.3a + 233.5b + 97.6c + 304.1d - 1109.0e + 4520.1\rho \quad (3)$$

where P_{CJ} is the detonation pressure [GPa]; D is the detonation velocity [m s^{-1}].

Table 2 shows detonation pressure and velocity estimated by empirical Equations and KHT code and a comparison with the experimental values. The predicted detonation pressure and velocity in Equation (2) and Equation (3) are in agreement with the experimental values. With an increase in the percentage of aluminum, the detonation pressure and velocity decreased gradually. The predicted detonation pressures obtained by the KHT code, considering that the aluminum powder was inert, are greater than the measured ones. The consistency between the predicted and measured detonation velocities is satisfactory. Combustion of aluminum powder in the explosives is assumed to occur during the expansion of gaseous detonation products. As the aluminum powder does not participate in the reaction zone, the detonation pressure and velocity decrease. To analyze the effect of explosive components, we expressed the detonation performance by the Al/O ratio. The linear correlations for detonation pressure and detonation velocity with Al/O ratio can be expressed as follows:

$$P_{CJ} = 24.858 - 2.189x \ (0 \le x \le 1.523) \quad (3)$$

$$D = 8556.996 - 614.668x \ (0 \le x \le 1.523) \quad (4)$$

Table 2. Results of the detonation parameters of HMX-based aluminized explosives.

No.	P_{CJ} [GPa]					D [m s^{-1}]					Q_v [kJ kg^{-1}]		
	Exp.	Eqs [2].	Dev. [%]	KHT[a)]	Dev. [%]	Exp.	Eqs [3].	Dev. [%]	KHT[a)]	Dev. [%]	Exp.	KHT[b)]	Dev. [%]
0	39.00	39.30	0.76	38.10	−2.3	9010	9160.00	1.66	9091	0.9	5530.0	5987.90	8.3
1	25.60	27.10	5.86	29.69	16.0	8584	8545.86	−0.44	8223	−4.2	5590.3	5773.27	1.0
2	24.33	25.80	6.04	28.69	17.9	8452	8312.94	−1.65	8066	−4.6	6173.9	6125.56	−0.8
3	23.68	24.59	3.84	26.21	10.7	8313	8093.59	−2.64	7897	−5.0	6832.5	6827.71	−0.1
4	23.14	23.37	0.99	25.82	11.6	8141	7865.19	−3.39	7687	−5.6	7290.5	7319.30	0.4
5	22.37	22.28	−0.40	23.98	7.2	7969	7659.4	−3.89	7460	−6.4	7267.6	7248.98	−0.3
6	21.97	21.08	−4.05	22.26	1.3	7621	7417.44	−2.67	7531	−1.2	6985.2	7015.29	0.4

a) Assuming that the Al particle is inert. b) Assuming that 47.2%, 58.0%, 56.6%, 49.9%, and 42.8% of the Al particle is active for formulas 2, 3, 4, 5, and 6, respectively.

where x is the Al/O ratio. The fitting curves are shown in Figure 4. The R-squared values of the correlation are 0.841 and 0.995, respectively.

Figure 5 shows the detonation heat of explosives as a function of the Al/O ratio. When the Al/O ratio equals

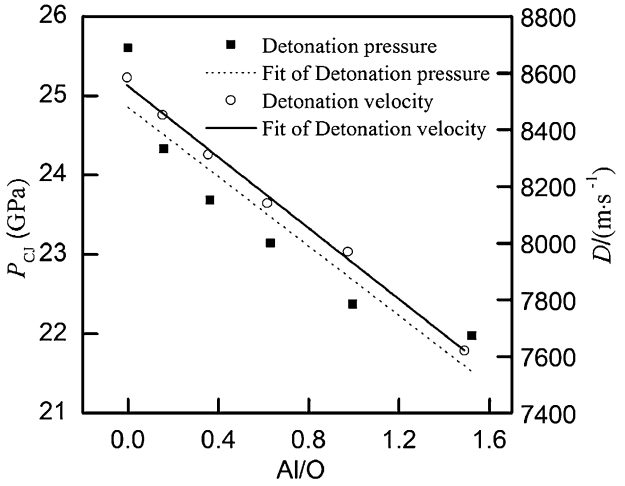

Figure 4. Variation of detonation pressure and detonation velocity with the Al/O ratio.

0.663, the detonation heat of explosives has a maximum value, which means an increase of 31.8% compared with that of explosives without aluminum particle. However, when the Al/O ratio further increases, the detonation heat begins to decrease. As shown in Figure 5, the predicted detonation heat is unreasonable whether the aluminum powder is inert or active, unless it assumes a certain proportion of the aluminum particle combusted in a detonation product, which is in agreement with the view of Deiter and Wilmot [25]. The HMX-based aluminized explosives studied in this paper have a threshold value of the contribution of Al powder to the detonation heat of about 31.8%.

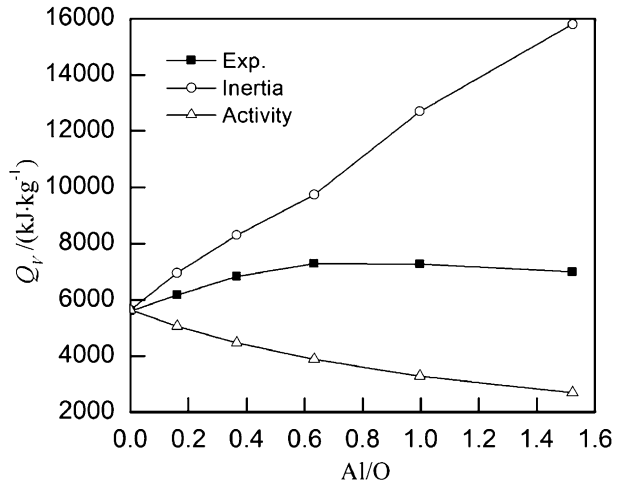

Figure 5. Variation of detonation heat with the Al/O ratio.

3 UNDEX Experiments

3.1 Experimental Setup

Six experiments were conducted to investigate the UNDEX performance of HMX-based aluminized explosives in a cylindrical water pool with a diameter of 85.0 m and a depth of 14.5 m. A schematic of the setup is shown in Figure 6. Six

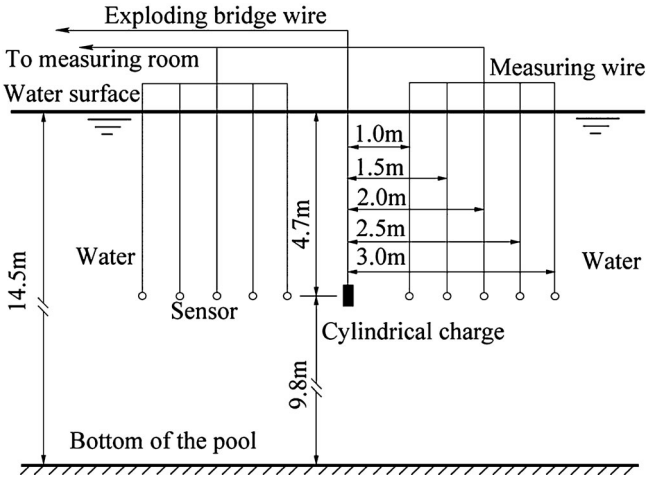

Figure 6. UNDEX experimental setup.

1 kg cylindrical charges of HMX-based aluminized explosives were detonated in tap water at a depth of 4.7 m, and 10 sensors were placed 1.0 m, 1.5 m, 2.0 m, 2.5 m, and 3.0 m from the center of the explosive facing the shock front. The ratio of length to diameter of the cylindrical charges ranged from 1:1 to 1.2:1, and the charges were detonated in the end face center using 10 g JH-14 booster charge. The error of the system was about 7.4%.

3.2 Results

Figure 7 shows the shock wave and the bubble pulse at 1 m for formula 2 during the underwater explosion recorded in pressure-time history at the sensor (300 ms pressure history and within 5.0 ms in the inserted graph). The incident shock wave arrived at 2.7 ms, with a peak value of 55.801 MPa, and then decayed rapidly at about 3 ms. The shock wave followed at about 260.2 ms after the first bubble pulse, with a broader profile and a lower maximum pressure. The period of the bubble pulse was 260.2 ms.

Table 3 shows the detailed results of the experiment for different formulas of HMX-based aluminized explosives. The values in the table are the average values measured at the same measuring point distance. R is the distance between the center of the explosive and the measuring point [m];

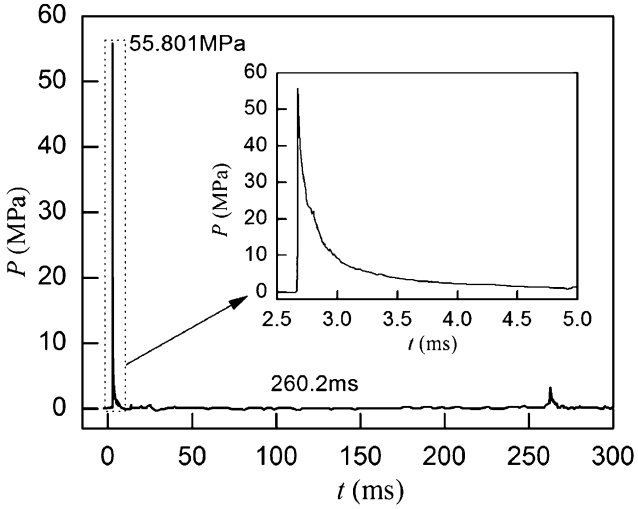

Figure 7. Typical pressure-time profiles of a 1.0 kg explosives for formula 2 at 1 m. The inserted graph shows the magnifying figures of the peak.

P_m is the peak pressure of shock wave [Pa]; T_b is the period of bubble [s]; θ is the attenuation time constant [μs], which is the time required by the peak pressure P_m to fall to P_m/e, and $e = 2.718$.

The calculation formula of the shock wave impulse (I), shock wave energy (E_s), shock wave energy flux density (E), and bubble energy (E_b) is expressed as [1]:

$$I(t) = \int_0^{6.7\theta} P(t)dt \tag{5}$$

$$E_s = \frac{4\pi R^2}{\rho_w C_w} \int_0^{6.7\theta} P^2(t)dt \tag{6}$$

$$E = \frac{1}{\rho_w C_w}(1 - 2.422\times10^{-4} P_m - 1.031 \times 10^{-8} P_m{}^2) \int_0^{6.7\theta} P^2(t)dt \tag{7}$$

$$E_b = 0.684 P_H^{5/2} T_b^3 \Big/ \rho_w^{3/2} \tag{8}$$

where $P(t)$ is the shock wave pressure [Pa], P_H is the hydrostatic pressure at charge [Pa], ρ_w is the water density [kg m^{-3}], C_w is the velocity of sound in water (C_w = 1450 m s^{-1}), and P_m is the peak pressure of shock wave [MPa].

As shown in Table 3, when the Al/O ratio increases, the peak pressure gradually decreases at the same measuring point for different formulas. When the Al/O ratio is equal to 0.366, the shock wave energy, flux density, and impulse at each measuring point reach the maximum value. The

Table 3. Results of UNDEX experiments of HMX-based aluminized explosive.

No.	Al/O	R [m]	P_m [MPa]	T_b [s]	E_s [MJ kg^{-1}]	E_b [MJ kg^{-1}]	E [MJ kg^{-1}]	I [kPa s^{-1}]	θ [μs]
1	0	1.0	55.913	0.2486	0.985	2.7714	0.0773	7205.7	82.4
		1.5	37.791		1.262		0.0442	4907.1	88.55
		2.0	26.491		1.100		0.0217	3277.2	93.39
		2.5	21.050		1.080		0.0137	2516.3	98.16
		3.0	18.646		1.065		0.0094	2371.3	100.03
2	0.161	1.0	55.801	0.2602	1.158	3.1777	0.0909	7584	86.82
		1.5	37.808		1.352		0.0474	5196.6	93.57
		2.0	26.424		1.225		0.0242	3561.5	96.07
		2.5	21.108		1.152		0.0146	2885.1	101.35
		3.0	18.691		1.146		0.0101	2576.5	104.62
3	0.366	1.0	54.413	0.2876	1.397	4.2910	0.1097	8171.6	93.64
		1.5	37.155		1.438		0.0504	5623.6	99.02
		2.0	26.334		1.327		0.0262	3950.6	102.42
		2.5	21.102		1.246		0.0158	3156.2	106.86
		3.0	18.678		1.233		0.0109	2870.8	108.34
4	0.633	1.0	52.604	0.3105	1.259	5.3998	0.0989	8679	98.04
		1.5	34.754		1.380		0.0484	5938.2	103.02
		2.0	26.386		1.274		0.0252	4272.6	108.85
		2.5	19.718		1.219		0.0154	3262.4	110.69
		3.0	17.513		1.162		0.0102	3045.2	113.53
5	0.997	1.0	48.753	0.3183	1.106	5.8170	0.0870	7863.6	99.31
		1.5	32.805		1.203		0.0422	5468.3	104.90
		2.0	24.201		1.176		0.0233	4021	109.07
		2.5	18.719		1.078		0.0137	3134.9	113.17
		3.0	16.612		1.066		0.0094	2896.4	115.04
6	1.523	1.0	40.584	0.3132	0.711	5.5418	0.0560	6179.8	100.61
		1.5	27.854		0.803		0.0282	4341.1	106.02
		2.0	20.098		0.735		0.0146	3152.1	109.55
		2.5	15.847		0.698		0.0089	2469.6	114.26
		3.0	14.297		0.683		0.0060	2316.3	115.36

bubble period and bubble energy reach their maximum values when the Al/O ratio equals 0.997, with an increase of 28% and 110% compared with the explosives without Al particle, respectively. However, the attenuation time constant gradually increases when the Al/O ratio increases.

Table 3 shows that a saturation value exists in the effect of the Al powder on the shock wave and the bubble. By adjusting the Al powder content in the explosives, anyone can devise explosives with different energy output structures for the UNDEX. For the HMX-based aluminized explosive studied in the paper, the content of the Al powder in the explosive should not exceed 30% to take the full advantage of the shock wave overpressure to damage the underwater targets, and the content of the Al powder should not exceed by 40% when the purpose is to take advantage of the low-frequency effects of the bubble pulse to achieve the overall damage of a ship. To achieve highly efficient damage, considering the target characteristics such as shape, size, and structure type, overpressure, and bubble pulsation should be comprehensively utilized.

3.3 Similar Laws of Shock Wave

For the mass of Q explosives detonated underwater, the peak pressure and attenuation time constant conform to the following power function form of similarity law equation, respectively:

$$P_m = K_1\ (R/Q^{1/3})^{\alpha} \tag{7}$$

$$\theta/Q^{1/3} = K_2\ (R/Q^{1/3})^{\beta} \tag{8}$$

The law of similarity coefficients is associated with explosives, K_1 and K_2 denote the magnitude of the parameter values of the UNDEX, and α and β denote the rate of change of the parameter value. The smaller the absolute value is the smaller rate of change of parameters.

Figure 8 and Figure 9 show that the measured peak pressure and attenuation time constant vs. $\ln(R/Q^{1/3})$ obtained good linear correlation, respectively.

The calculated coefficient of HMX-based aluminized explosives is given in Table 4. As shown in Figure 4, Figure 5, and Table 1, when increasing the Al/O ratio, the peak pressure is gradually decreased and the attenuation time constant gradually increases. The change rate of the pressure and time shows a decreasing trend.

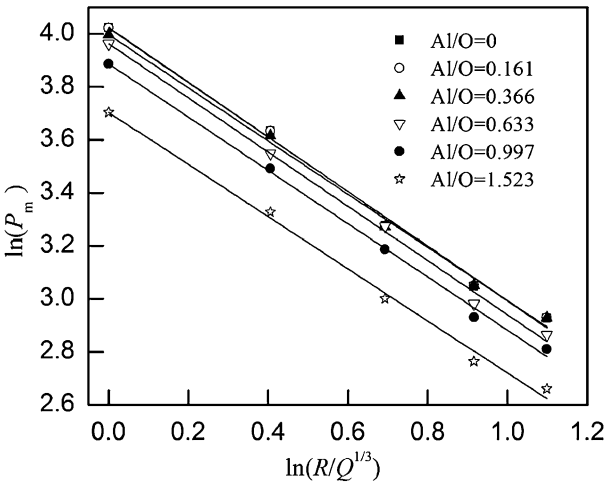

Figure 8. Peak pressure vs. scaled distance.

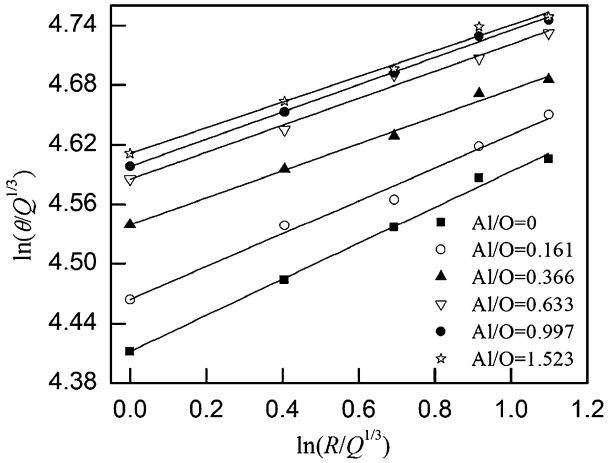

Figure 9. Attenuation time vs. scaled distance.

3.4 Simulation of the Bubble

Considering the theory of underwater explosion, an arbitrary aspect of partitioning the underwater explosion bubble

Table 4. Law of similarity coefficients for HMX-based aluminized explosives.

Al/O	Peak value of pressure [P_m]			Attenuation time constant [θ]		
	K_1 [MPa]	α	*Adj. R-square*	K_2 [μs]	β	*Adj. R-square*
0	55.92	1.032	0.993	82.40	−0.182	0.994
0.161	55.78	1.028	0.993	86.82	−0.166	0.982
0.366	54.42	1.003	0.994	93.64	−0.136	0.991
0.633	52.55	1.023	0.995	98.04	−0.136	0.985
0.997	48.62	1.005	0.996	99.31	−0.137	0.996
1.523	40.53	0.984	0.993	100.61	−0.129	0.987

phenomenology into shockwave and oscillation phases is defining their time of connection. Figure 10 shows that, using the law of similarity coefficients of the shock wave, the radius-time and the velocity-time curves of the initial bubbles for 1 kg HMX-based aluminized explosives detonated at a depth of 4.7 m can be derived according to the volume-acceleration model [26]. The radius of the bubble increases, and the radial velocity abruptly increases within 0.07 ms, before gradually decreasing with increasing time. When $t > 0.6$ ms, the radial velocity changes slowly.

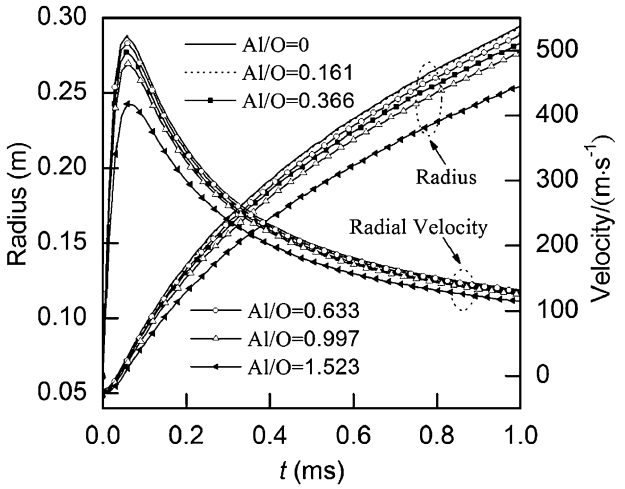

Figure 10. Time history of the radius and velocity of the bubble at a depth of 4.7 m.

Taking $t = 0.9$ ms as the initial bubble formation time, we use numerical simulation to study the bubble pulsation of UNDEX for HMX-base aluminized explosives using the nonlinear MSC.DYTRA finite element (FE) software. Based on the FE model, the dimensions of the water region are $10.0 \times 10.0 \times 10.0$ m^3, and those of the air region are $10.0 \times 2.0 \times 10.0$ m^3. The fluid elements in the FE models are represented using hexahedron elements (i.e., Eulerian elements with eight corner grid points). Two subroutines are developed to define the initial and boundary conditions in the fluid field [27].

The bubble's entire evolution in two periods, with developed subroutines as calculated by MSC.DYTRAN, is presented in Figure 11. During the expansion and early collapse, the calculated motion is in excellent agreement with that in a previous small-dose experiment [27]. As the detonation depth is greater than the maximum bubble radius, with the expansion of the bubble, only a small spray dome is formed on the free surface. The entire process of bubble pulsation, including the collapse and formation of the liquid jet, can be clearly and directly observed in the numerical simulation.

In Figure 12, the radius of the bubbles as a function of time is demonstrated in numerical results under the six-formula HMX-based aluminized explosive. With the increase in

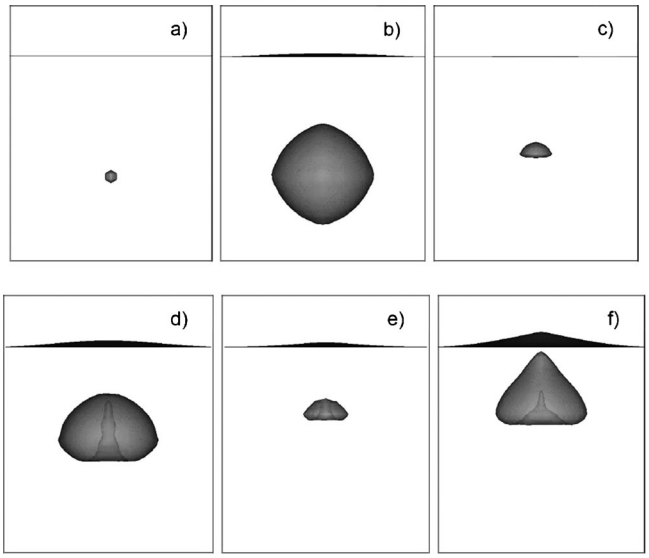

Figure 11. Typical evolution of the bubble for formula 1 at a depth of 4.7 m. (a) $t = 0$ ms, (b) $t = 124.1$ ms, (c) $t = 252.1$ ms, (d) $t = 392$ ms, (e) $t = 508$ ms, (f) $t = 592$ ms.

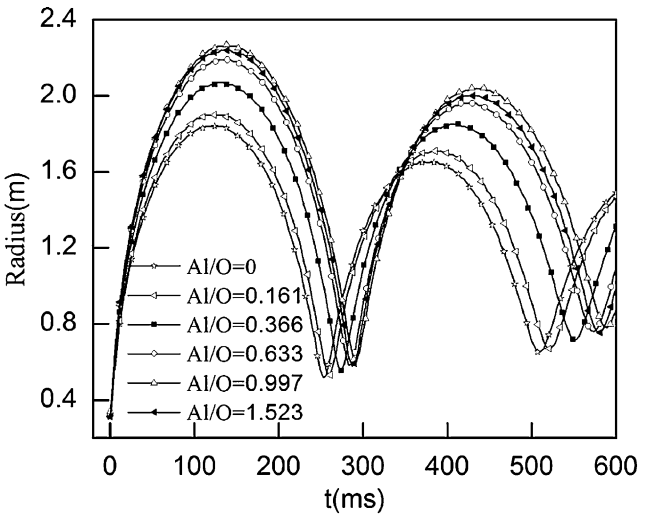

Figure 12. Radius-time history curve for a 1.0 kg explosive at a depth of 4.7 m.

the Al/O ratio, the maximum bubble radius and first bubble period show a maximum value, increasing by 17% and 23%, respectively, compared with those in the explosive without Al particle at ratio of 0.997. When the Al/O ratio increases to 1, the bubble radius and period start to decrease. This law is similar to the explosion heat with the variation of the Al/O ratio. The result shows that the detonation heat of the HMX-based explosive directly affects the bubble pulsation characteristics.

Table 5 reports the tested and numerical results for the period and max radius of the bubbles. The calculated results of the period of the bubble are in good agreement with the experimental data, with error of less than 10%. No

Table 5. Bubble parameters of HMX-based aluminized explosives.

Al/O	Period of bubble T_b			Max radius of bubble R_{bm}
	Exp. [ms]	FEA [ms]	Error [%]	FEA [m]
0	248.6	253	1.8	1.84
0.161	260.2	261	0.3	1.90
0.366	287.6	274	−3.7	2.07
0.633	310.5	283	−8.9	2.19
0.997	318.3	296	−7.0	2.27
1.523	313.2	287	−8.4	2.24

experiment results are available for the bubble radius. The only numerical result shows that when the Al/O ratio equals 1, the bubble maximum radius is about 2.27 m.

4 Conclusions

Detonation and UNDEX experiments were carried out to investigate the effect of the Al/O ratio on the performance of six HMX-based aluminized explosives. The experimental results obtained for the detonation pressures, velocities, and heat compared with the results calculated by an empirical formula and the KHT code were in good agreement. The detonation pressures and velocities decreased when the Al/O ratio in the HMX-based aluminized explosive increased, which indicates a linear relationship. Moreover, detonation heat had a tendency to increase first; subsequently, a parabolic decrease was observed when further increasing the Al/O ratio. At an Al/O ratio of 0.997 (i.e., 40% aluminum content), the detonation heat reached a maximum value of 31.8% compared with that in the explosive without Al particle.

The effects of the Al/O ratio on the shock wave pressure and bubble of UNDEX were analyzed. The results showed that when the Al/O ratio increases, the shock wave peak pressure increases and then decreases. When the Al/O ratio equals 0.366, the shock wave energy, energy flux density, and impulse at each measuring point reach a maximum value. When the Al/O ratio equals 0.997, the detonation heat increases, and the bubble period and radius attain maximum values of 318.3 ms and 2.27 m, respectively.

For the HMX-based aluminized explosives studied in this paper, different underwater energy output structures were realized by adjusting the Al content. The Al/O ratio should be controlled at less than 0.997, and the optimum ratio should be between 0.366 and 0.633; that is, the Al content should be controlled in the range of 20% to 30%.

Acknowledgments

The authors would like to express their gratitude to Dr. Xiao-jun Feng and Dr. Hao Wang, whose efforts were essential to the detonation experiments. This research was supported by the National Natural Science Foundation of China (Project Nos. 11272057 and 51209042).

References

[1] R. H. Cole, *Underwater Explosion*, Princeton University Press, New Jersey **1948**.
[2] M. H. Keshavarz, R. T. Mofrad, K. E. Poor, A. Shokrollahi, A. Zali, M. H. Yousefi, Determination of Performance of Non-ideal Aluminized Explosives, *J. Hazard. Mater.* **2006**, *137*, 83.
[3] M. H. Keshavarz, R. H. Motamedoshariati, R. Moghayadnia, H. R. Nazari, J. Azarniamehraban, A New Computer Code to Evaluate Detonation Performance of High Explosives and their Thermochemical Properties, Part I, *J. Hazard. Mater.* **2009**, *172*, 1218.
[4] W. C. Strahle, *Investigation of Research Requirements for Underwater Explosion*, Report ADA-230840, Georgia Inst of Tech Atlanta School of Aerospace Engineering, Atlanta, GA, USA, **1990**.
[5] D. A. Cichra, R. M. Doherty, Estimation of Performance of Underwater Explosives, *9th Symposium on Detonation*, Portland, OR, USA, August 27–September 1, **1989**.
[6] C. L. Mader, *Detonation Properties of Condensed Explosives Computed Using the Becker-Kistiakosky-Wilson Equation of State*, Report LA-2900, Los Alamos National Laboratory, Los Alamos, NM, USA, **1963**.
[7] M. Cowperthwaite, W. H. Zwisler, The JCZ Equations of State for Detonation Products and Their Incorporation into the TIGER Code, *6th International Symposium on Detonation*, Coronado, CA, USA, August 24–27, **1976**.
[8] K. Tanaka, Detonation Properties of High Explosives Calculated by Revised Kihara-Hikita Equation of State, *8th International Symposium on Detonation*, Albuquerque, NM, USA, July 15–19, **1985**.
[9] J. W. Kury, H. C. Hornig, E. L. Lee, Metal Acceleration by Chemical Explosives, *4th International Symposium on Detonation*, Silver Spring, MD, USA, October 12–15, **1965**.
[10] R. Rajendran, K. Narasimhan, Deformation and Fracture Behavior of Plate Specimens Subjected to Underwater Explosion: A Review, *Int. J. Impact Eng.* **2006**, *32*, 1945.
[11] R. Rajendran, Numerical Simulation of Underwater Explosion Bulge Test, *Mater. Des.* **2009**, *30*, 4335.
[12] R. Rajendran, Numerical Simulation of Response of Plane Plates Subjected to Primary Shock Loading of Non-contact Underwater Explosion, *Mater. Des.* **2009**, *30*, 1000.
[13] C. Y. Jen, Y. S. Tai, Deformation Behavior of a Stiffened Panel Subjected to Underwater Shock Loading Using the Non-linear Finite Element Method, *Mater. Des.* **2010**, *31*, 325.
[14] C. F. Hung, P. Y. Hsu, J. J. Hwang-Fuu, Elastic Shock Response of an Air-backed Plate Subjected to Underwater Explosion, *Int. J. Impact Eng.* **2005**, *31*, 151.
[15] C. F. Hung, B. J. Lin, J. J. Hwang-Fuu, P. Y. Hsu, Dynamic Response of Cylindrical Shell Structures Subjected to Underwater Explosion, *Ocean Eng.* **2009**, *36*, 564.
[16] K. Ramajeyathilagam, C. P. Vendhan, R. V. Bhujanga, Non-linear Transient Dynamic Response of Rectangular Plates under Shock Loading, *Int. J. Impact Eng.* **2000**, *24*, 999.
[17] K. Ramajeyathilagam, Deformation and Rupture of Thin Rectangular Plates Subjected to Underwater Shock, *Int. J. Impact Eng.* **2004**, *30*, 699.
[18] R. C. Batra, N. M. Hassan, Response of Fiber Reinforced Composites to Underwater Explosive Loads, *Composites Part B* **2007**, *38*, 448.
[19] L. Librescu, S. Y. Oh, J. Hohe, Dynamic Response of Anisotropic Sandwich Flat Panels to Underwater and In-air Explosions, *Int. J. Solid Struct.* **2006**, *46*, 3794.

[20] W. H. Lai, Transient Dynamic Response of Submerged Sphere Shell with an Opening Subjected to Underwater Explosion, *Ocean Eng.* **2007**, *34*, 653.
[21] M. M. Swisdak Jr., *Explosion Effects and Properties. Part II. Explosion Effects in Water*, Report ADA-056694, Naval Surface Weapons Center White Oak Lab, Silver Spring MD, USA, **1978**.
[22] E. Stromsoe, S. Eriksen, Performance of High Explosives in Underwater Applications. Part 2: Aluminized Explosives, *Propellants Explos. Pyrotech.* **1990**, *15*, 52.
[23] N. Masahiko, A. Aoki, H. Miyoshi, Effects of Aluminum on the Energy of Underwater Explosion for the Insensitive PBXs, *Insensitive Munitions of Technology Symposium*, San Diego, CA, March 19–21, **1996**.
[24] T. Keicher, Influence of Aluminium/Ammonium Perchlorate on the Performance of Underwater Explosives, *Propellants Explos. Pyrotech.* **1999**, *24*, 140.
[25] J. S. Deiter, G. B. Wilmot, Detonation Chemistry of Underwater Explosives, *10th International Symposium on Detonation*, Boston, MA, USA, July 12–16, **1993**.
[26] K. S. Hunter, *Global-shape-function Models of an Underwater Explosion Bubble*, Faculty of Graduate School of the University of Colorado, Department of Mechanical Engineering, Boulder, CO, USA, **2001**.
[27] J. Li, J. L. Rong, Bubble and Free Surface Dynamics in Shallow Underwater Explosion, *Ocean Eng.* **2011**, *38*, 1861.
[28] E. Klaseboer, K. C. Hung, C. Wang, C. W. Wang, B. C. Khoo, P. Boyce, S. Debono, H. Charlier, Experimental and Numerical Investigation of the Dynamics of an Underwater Explosion Bubble Near a Resilient/rigid Structure, *J. Fluid Mech.* **2005**, *537*, 387.

Received: March 3, 2013
Revised: May 15, 2013
Published online: August 13, 2013

